JBC RESEARCH ARTICLE

TFEB insufficiency promotes cardiac hypertrophy by blocking autophagic degradation of GATA4

Received for publication, March 15, 2021, and in revised form, September 3, 2021 Published, Papers in Press, September 10, 2021,
https://doi.org/10.1016/j.jbc.2021.101189

Rui Song[1,2], **Han Lei**[3], **Li Feng**[4], **Wanwen Cheng**[1], **Ying Li**[1], **Ling Ling Yao**[5,*], **and Jie Liu**[1,*]

From the [1]*Department of Pathophysiology, Guangdong Key Laboratory of Genome Stability and Human Disease Prevention, Shenzhen University Health Science Center, Shenzhen, China;* [2]*College of Physics and Optoelectronic Engineering, Shenzhen University, Shenzhen, China;* [3]*Department of Physiology and Pathophysiology, School of Basic Medical Sciences, Fudan University, Shanghai, China;* [4]*Department of Cardiology, Zhongshan People's Hospital, Guangzhou, China;* [5]*Department of Cardiology, First Affiliated Hospital, Guangdong College of Pharmacy, Guangzhou, China*

Edited by Ronald Wek

Autophagosome–lysosome pathway (ALP) insufficiency has been suggested to play a critical role in the pathogenesis of cardiac hypertrophy. However, the mechanisms underlying ALP insufficiency remain largely unknown, and strategies to specifically manipulate ALP insufficiency for treating cardiac hypertrophy are lacking. Transcription factor EB (TFEB), as a master regulator of ALP, regulates the generation and function of autophagosomes and lysosomes. We found that TFEB was significantly decreased, whereas autophagosome markers were increased in phenylephrine (PE)-induced and transverse aortic constriction–induced cardiomyocyte hypertrophy and failing hearts from patients with dilated cardiomyopathy. Knocking down TFEB induced ALP insufficiency, as indicated by increased autophagosome markers, decreased light chain 3II flux, and cardiomyocyte hypertrophy manifested through increased levels of atrial natriuretic peptide and β-myosin heavy chain and enlarged cell size. The effects of TFEB knockdown were abolished by promoting autophagy. TFEB overexpression improved autophagic flux and attenuated PE-stimulated cardiomyocyte hypertrophy and transverse aortic constriction–induced hypertrophic remodeling, fibrosis, and cardiac dysfunction. Curcumin analog compound C1, a specific TFEB activator, similarly attenuated PE-induced ALP insufficiency and cardiomyocyte hypertrophy. TFEB knockdown increased the accumulation of GATA4, a transcription factor for several genes causing cardiac hypertrophy by blocking autophagic degradation of GATA4, whereas knocking down GATA4 attenuated TFEB downregulation–induced cardiomyocyte hypertrophy. Both TFEB overexpression and C1 promoted GATA4 autophagic degradation and alleviated PE-induced cardiomyocyte hypertrophy. In conclusion, TFEB downregulation plays a vital role in the development of pressure overload–induced cardiac hypertrophy by causing ALP insufficiency and blocking autophagic degradation. Activation of TFEB represents a potential therapeutic strategy for treating cardiac hypertrophy.

Autophagy is an evolutionarily conserved pathway that directs cytoplasmic components, including organelles, protein aggregates, and individual proteins, to the lysosome for degradation. The basal level of autophagy is essential for maintaining intracellular homeostasis, and impaired or hyperactive autophagy disturbs cellular function and induces disease. Three forms of autophagy have been identified: macroautophagy, microautophagy, and chaperone-mediated autophagy. Macroautophagy, also known as the autophagosome–lysosome pathway (ALP), involves autophagosome formation, autophagosome–lysosome fusion (or autophagosome maturation), and lysosome degradation and induces the bulk degradation of cellular content. Microautophagy involves only lysosome that captures and degrades a small amount of soluble cytoplasmic content, whereas in the selective chaperone-mediated autophagy, the lysosome takes in specific protein molecules individually for degradation with the aid of an adaptor protein (1). Macroautophagy or ALP is the most extensively studied of these, particularly with regard to diseases, such as neurodegenerative disease, metabolic syndrome, and cardiovascular diseases (2–8).

Pathological cardiac hypertrophy and remodeling, initially an adaptive response of the heart to pressure or volume overload, are fundamental morphological changes in the progression of heart failure (HF), a leading cause of death worldwide (9–11). Inhibition of pathological remodeling represents a promising therapeutic strategy to reduce morbidity and mortality from HF. Studies have investigated the initiation of autophagy under the stress of pressure overload (PO), the most common cause of cardiac hypertrophy, and the possible contribution of autophagy to the pathological remodeling of the heart. Despite contradictory conclusions, the more recent reports overwhelmingly support the participation of ALP insufficiency in the pathological remodeling of myocardial hypertrophy (12–17). An earlier study demonstrated increased microtubule-associated protein 1 light chain 3 (LC3)–positive autophagosome formation and upregulated expression of beclin-1, a protein promoting autophagosome formation, in transverse aortic constriction (TAC)–induced cardiac hypertrophy and HF. The TAC-induced increase in autophagosome

* For correspondence: Ling Ling Yao, yaolingling1979@gmail.com; Jie Liu, liuj@szu.edu.cn.

abundance and cardiac dysfunction were largely ameliorated in beclin-$1^{+/-}$ mice, which led the authors to the conclusion that enhanced autophagy has a detrimental effect in PO-induced cardiac hypertrophy (18). However, another study showed that administration of Tat-beclin-1, a potent small-peptide inducer of autophagy derived from a region of beclin-1 that enhances autophagy, attenuated PO-induced pathological changes (13). The controversial conclusion from the genetic and pharmacological manipulation of beclin-1 has been attributed to the various complicated effects of beclin-1 on autophagic flux, which depend on which partners it forms a complex with (19). The genetic manipulation of beclin-1 might have impaired autophagic flux. Growing evidence indicates that myocardial ALP insufficiency, rather than autophagosome formation, occurs in PO-induced cardiac hypertrophy. Manipulations promoting autophagosome formation are detrimental to the treatment of cardiac hypertrophy. For example, enhancing beclin-1–mediated autophagy by miR30a knockdown (KD) exacerbates PO-induced cardiac hypertrophy, fibrosis, and HF (20), whereas treatment with 3-methyladenine to stop the formation of autophagosomes ameliorated PO-induced cardiac pathology (21). Conversely, strategies improving ALP activity, such as the application of mechanistic target of rapamycin kinase complex 1 (mTORC1) inhibitors (*i.e.*, rapamycin and its analogs) and AMP-activated protein kinase activators (*i.e.*, 5-amino-4-imidazole-1-β-D-carboxamide ribofuranoside, metformin, or R118), which activate autophagy flux by activating UNC51-like kinase directly or *via* mTORC1 inactivation, are beneficial in the treatment of cardiac hypertrophy and HF (19). In addition, the changes in autophagy during the development of cardiac hypertrophy are likely to be time dependent, where autophagic flux has been shown to increase at the very early stage of the disease (3–12 h after TAC), and then decreased gradually (13). Therefore, how and when autophagy should be modulated is a critical concern in the treatment of pathological cardiac hypertrophy. Improving ALP is a potential therapeutic strategy against pathological remodeling. However, the mechanisms underlying the ALP insufficiency in cardiac hypertrophy remain largely unknown, and the measures taken to improve cardiac ALP are often nonspecific as a result (1).

Transcription factor EB (TFEB), a member of the microphthalmia family transcription factors (TFs) with a basic helix–loop–helix leucine-zipper structure, was recently identified as a key regulator, orchestrating the whole ALP process (22). TFEB directly regulates both the production and functions of the lysosome and also the generation and maturation of autophagosomes (22–25). Enforced TFEB expression has been suggested to have a therapeutic effect on diseases associated with lysosomal or ALP insufficiency, including the accumulation of aberrant aggregates, that is, neurodegenerative diseases such as Parkinson's disease, Alzheimer's disease, and Huntington's disease (24, 26–29); and liver damage and pulmonary fibrosis caused by the accumulation of misfolded proteins (30, 31). TFEB-mediated autophagy is also known to contribute to glycolipid, doxorubicin, and protein accumulation–induced heart toxicity and ischemic reperfusion injury, and TFEB activation can alleviate myocardial damage (32–36).

Despite the beneficial effect of TFEB on the treatment of those diseases, TFEB can be harmful to normal organ functions. For example, heart-specific TFEB overexpression impairs cardiac function and induces cardiomyopathy in TFEB transgenic mice (37). The detrimental effects of TFEB have also been observed in transgenic mice with neuron-specific TFEB overexpression (38). However, adeno-associated virus (AAV)-mediated moderate TFEB overexpression is not harmful to these organs (29, 35, 39–41). Therefore, TFEB is likely to exert controversial effects under normal and diseased conditions, depending on TFEB expression levels and pathological features of the disease. In addition, endothelial cell-, adipocyte-, and macrophage-specific TFEB transgenic mice show no damaged symptoms (42–44), suggesting the effect of TFEB has tissue specificity. PO-induced cardiac hypertrophy has prominent pathological features distinguished from those reported heart diseases whose developments are associated with TFEB activity. So far, no studies have established the link between TFEB and pathological remodeling in the context of cardiac hypertrophy. The study on TFEB in the context of pathological cardiac hypertrophy can provide new insight into the mechanism underlying this disease. It is of particular significance to explore the therapeutic potential of targeting TFEB for the treatment of cardiac hypertrophy.

In this study, we investigated whether and how TFEB modulates autophagy in PO-induced cardiac hypertrophy and the possible role of TFEB in the pathological remodeling. For this purpose, we examined TFEB expression and activity in a cell model of PE-stimulated cardiomyocyte hypertrophy and a mouse model of TAC-induced cardiac hypertrophy. By manipulating TFEB expression, we investigated the role and mechanisms of TFEB in regulating autophagy in cardiac hypertrophy and TFEB-mediated autophagy in the pathological remodeling. Finally, we activated TFEB genetically and pharmacologically to explore the possible therapeutic effects of TFEB on cardiac hypertrophy.

Results

TFEB expression is downregulated, and autophagic flux is blocked in pathological cardiac hypertrophy

First, we explored changes in TFEB expression and autophagy in phenylephrine (PE; 50 μmol/l, 48 h)-induced cardiomyocyte hypertrophy and TAC (8 weeks)-induced mouse cardiac hypertrophy models. The mRNA levels of natriuretic peptide precursor A (NPPA) and natriuretic peptide precursor B (NPPB), biomarkers of cardiac hypertrophy, were significantly increased in the cell and animal cardiac hypertrophy models (Fig. 1, *A* and *B*). TFEB mRNA and protein levels were significantly decreased in hypertrophic cardiomyocytes and TAC-mice heart tissues compared with controls (Fig. 1, *A*, *B*, *D*, and *E*). In contrast, the protein levels of LC3 type II (microtubule-associated protein 1 LC3 type II) and, especially, P62 were increased in PE-stimulated cardiomyocytes and TAC hearts (Fig. 1, *G* and *H*), indicative of the blocking of

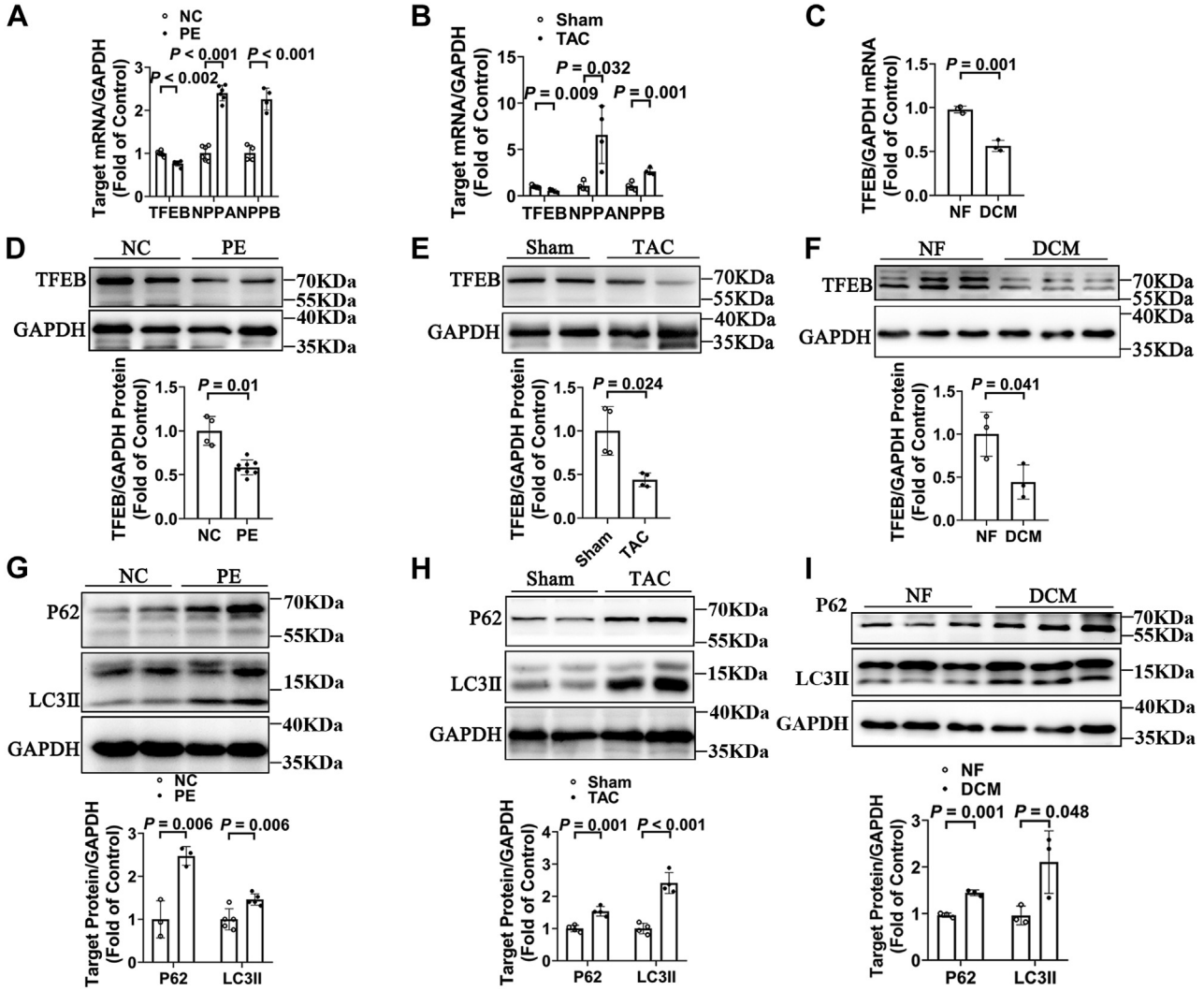

Figure 1. Transcription factor EB (TFEB) expression is downregulated, and autophagic flux is blocked in pathological cardiac hypertrophy. *A*, statistics of TFEB, natriuretic peptide precursor A (NPPA), and natriuretic peptide precursor B (NPPB) mRNA levels in neonatal rat ventricular myocytes (NRVMs) treated with or without phenylephrine (PE; 50 μmol/l, 48 h). n = 4 to 6. Data represent mean ± SD from three independent experiments. *B*, statistical data of TFEB, NPPA, and NPPB mRNA levels in hearts from sham or transverse aortic constriction (TAC) mice. n = 4. Data represent mean ± SD from three independent experiments. *C*, statistics of TFEB mRNA levels in hearts from patients with dilated cardiomyopathy (DCM). n = 3. Data represent mean ± SD. *D* and *G*, representative immunoblots and statistical data of TFEB, P62, and microtubule-associated protein 1 light chain 3 type II (LC3II) protein levels in NRVMs treated with or without PE (50 μmol/l, 48 h). n = 3 to 8. Data represent mean ± SD from at least three independent experiments. *E* and *H*, representative immunoblots and statistics of TFEB, P62, and LC3II protein levels in heart tissues from sham or TAC mice. n = 4. Data represent mean ± SD from three independent experiments. *F* and *I*, representative immunoblot images and statistical data of TFEB, P62, and LC3II protein levels in human hearts from adult donors (nonfailing, NF) and patients with DCM. n = 3. Data represent mean ± SD.

autophagic flux in cardiac hypertrophy. Furthermore, we found similarly decreased TFEB and increased LC3II and P62 protein levels in human hearts isolated from patients with dilated cardiomyopathy compared with healthy human heart tissues (Fig. 1, *C*, *F*, and *I*). The data collectively indicate that TFEB expression is decreased, and autophagic flux is blocked in pathological cardiac hypertrophy.

TFEB downregulation induces cardiomyocyte hypertrophy by blocking autophagic flux

To explore the possible role of TFEB in the development of cardiac hypertrophy, we performed TFEB KD in neonatal rat ventricular myocytes (NRVMs) by RNA interference adenovirus (multiplicity of infection [MOI] = 30, 60 h) to simulate the change in TFEB associated with pathological cardiac hypertrophy. Decreased TFEB expression remarkably increased the protein levels of atrial natriuretic peptide (ANP) and myosin heavy chain-β (β-MHC), and NRVM cell size when compared with control cells (mCherry; Fig. 2, *A* and *B*), suggesting there is a causal relationship between decreased TFEB and the pathogenesis of cardiomyocyte hypertrophy.

Next, we examined how TFEB KD affects autophagic flux in NRVMs. We found that protein levels of both LC3II and P62 were significantly increased in TFEB-KD cells compared with mCherry controls (Fig. 2*C*). While LC3II protein levels reflect the abundance of

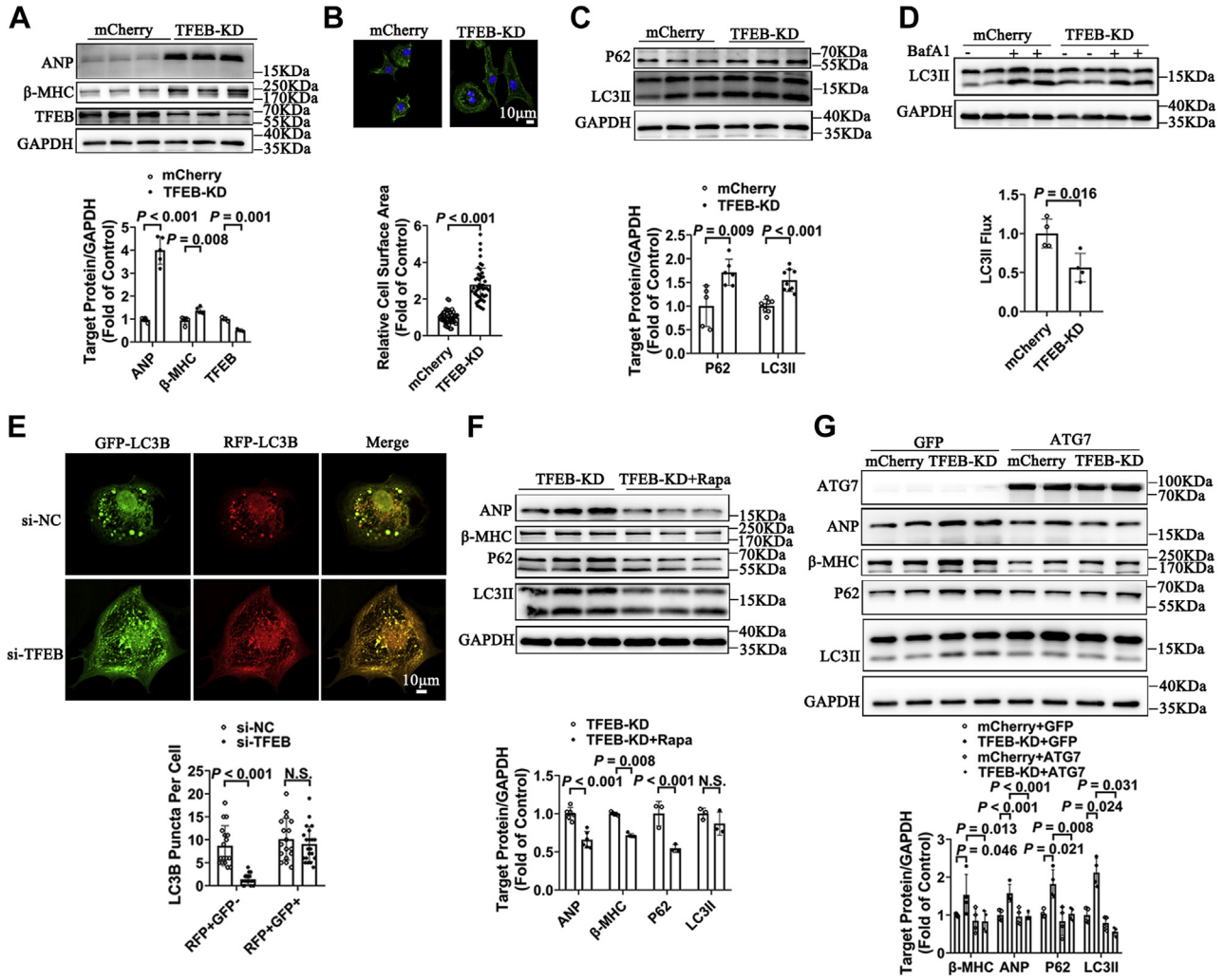

Figure 2. Transcription factor EB (TFEB) downregulation induces cardiomyocyte hypertrophy by blocking autophagic flux. *A*, representative immunoblots and statistics of atrial natriuretic peptide (ANP), myosin heavy chain-β (β-MHC), and TFEB protein levels in neonatal rat ventricular myocytes (NRVMs) infected with mCherry or TFEB knockdown (TFEB-KD) adenoviruses. n = 3 to 5. Data represent mean ± SD from at least three independent experiments. *B*, representative images and statistics of the cell-surface area of mCherry control and TFEB-KD NRVMs. n = 45 to 47 cells from four animals. Data represent mean ± SD from three independent experiments. *C*, representative immunoblots and statistics of P62 and microtubule-associated protein 1 light chain 3 type II (LC3II) protein levels in NRVMs. The blot of GAPDH was the same as that in *A*, as the blots of target protein in the two figures were taken from the same samples in the meantime. n = 5 to 8. Data represent mean ± SD from four independent experiments. *D*, representative immunoblots of LC3II protein levels and statistics of LC3II flux in NRVMs infected with mCherry or TFEB-KD adenoviruses with or without BafA1 (bafilomycin; 50 nmol/l, 6 h) treatment. The calculation was as described in the Experimental procedures section. n = 4. Data represent mean ± SD from three independent experiments. *E*, representative images of NRVMs infected with LC3B tandemly tagged with an acid-resistant monomeric red fluorescent protein (RFP) and acid-sensitive GFP (mRFP-GFP-LC3B) adenovirus treated with negative control (NC) siRNA or TFEB siRNA and quantification of LC3B puncta; n = 17 to 21 cells from three animals. Data represent mean ± SD from three independent experiments. *F*, representative immunoblots and statistics of ANP, β-MHC, P62, and LC3II protein levels in TFEB-KD NRVMs treated with or without rapamycin (Rapa; 20 μmol/l, 36 h). n = 3 to 6. Data represent mean ± SD from three independent experiments. *G*, representative immunoblots and statistics of autophagy-relative protein 7 (ATG7), ANP, β-MHC, P62, and LC3II protein levels in TFEB-KD NRVMs infected with GFP or ATG7 (MOI = 20, 48 h). n = 4. Data represent mean ± SD from three independent experiments. MOI, multiplicity of infection; N.S., not significant.

autophagosomes, the rate of LC3II degradation (*i.e.*, LC3II flux) indicates the degradation rate of autophagosomes by the lysosome (*i.e.*, autophagic flux) (45). The LC3II flux, as measured by the net amount of LC3II accumulated by bafilomycin A1 (BafA1; 50 nmol/l, 6 h) induced lysosomal inhibition was remarkably decreased in TFEB-KD NRVMs (Fig. 2*D*). Furthermore, TFEB KD decreased red fluorescent protein $(RFP)^+$ GFP^- puncta of LC3B, indicating the formation of autophagolysosomes (Fig. 2*E*). The results consistently provided evidence for the blockage of autophagic flux in TFEB-KD NRVMs.

As autophagy is important to preserve metabolic capacity by removing damaged mitochondria, we explored the effects of TFEB KD on mitochondrial biological activities. TFEB downregulation significantly decreased the protein levels of peroxisome proliferator–activated receptor-gamma coactivator-1α (PGC1α) and mitochondrial import receptor subunit TOM20 homolog (Tomm20), the biomarkers for mitochondria biogenesis and mitochondria content, respectively (Fig. S4*A*). Meanwhile, mitochondrial activity measured with WST-1 assay was decreased in TFEB-KD cells compared with control cells (Fig. S4*B*). Consistently, ATP production in

TFEB-KD cells was significantly decreased (Fig. S4*C*). Furthermore, we found that TFEB KD decreased mitochondrial membrane potential (Fig. S4*D*) and increased mitochondrial superoxide production (Fig. S4*E*). These results collectively indicate that TFEB KD induces damages to mitochondrial biogenesis, activity, and function.

Furthermore, we determined how autophagic-flux blockage contributes to TFEB-induced cardiac hypertrophy. mTORC1 is a negative regulator of autophagy flux (19). We used rapamycin (20 μmol/l, 36 h) to inhibit mTORC1 activity to examine its effect on TFEB-induced hypertrophy. The results show that rapamycin decreased the protein levels of LC3II and P62 in TFEB-KD cells, suggesting there was an improvement in autophagic flux. The expression levels of the hypertrophic markers ANP and β-MHC were also significantly decreased (Fig. 2*F*), suggesting TFEB downregulation induces cardiomyocyte hypertrophy by blocking autophagic flux. Considering that rapamycin is also a potent inhibitor for protein synthesis and metabolic activities in addition to regulating autophagy, we manipulated cellular autophagy activity more specifically by transfecting the cells with autophagy-related protein 7 (ATG7)–carrying adenovirus (MOI = 20, 48 h) 12 h after transfection of TFEB-KD adenovirus. Consistent with the result of rapamycin, ATG7 overexpression decreased TFEB-KD–induced increase in protein levels of P62 and LC3II, as well as ANP and β-MHC (Fig. 2*G*), confirming autophagic flux blockade contributes to cardiomyocyte hypertrophy by TFEB downregulation.

TFEB downregulation inhibits GATA4 autophagic degradation

Consistent with its effect on ANP and β-MHC protein levels, TFEB downregulation dramatically increased mRNA levels of NPPA and myosin heavy chain 7B (MYH7B) that encode ANP and β-MHC, respectively (Fig. 3*A*), implicating the involvement of prohypertrophic TF(s) that control fetal gene transcription. GATA4 is such a TF upregulating the expression of several cardiac-specific fetal genes that promote cardiomyocyte growth and plays an essential role in the pathogenesis of cardiac hypertrophy (46, 47). A recent study reported that GATA4 accumulated in senescent lung tissue because its autophagy-mediated degradation was inhibited, which promoted inflammation and senescence (48). No studies have investigated the possible role of autophagy in regulating GATA4 protein stability in cardiomyocytes. Therefore, we hypothesized that TFEB KD controls GATA4 protein levels by changing its degradation rate through regulating autophagic flux. To test this, we examined the protein levels of GATA4 in TFEB-KD cells and found them to be significantly increased (Fig. 3*B*). In contrast, GATA4 mRNA levels were decreased in TFEB-KD NRVMs, suggesting TFEB upregulates GATA4 at the protein level (Fig. 3*C*). Blocking the ALP with chloroquine (CQ; 20 μmol/l, 24 h) and bafilomycin (BafA1; 50 nmol/l, 6 h) significantly increased basal GATA4 protein levels (Fig. 3*D*), whereas enhancing autophagy flux with rapamycin decreased GATA4 protein levels (Fig. 3*E*) in TFEB-KD NRVMs. All our findings led us to the conclusion that, in cardiomyocytes, GATA4 stability is regulated by autophagy, and TFEB increases GATA4 autophagic degradation.

To address whether GATA4 accumulation accounts for TFEB downregulation–induced cardiac hypertrophy, we knocked down GATA4 expression in cardiomyocytes using GATA4 siRNA and observed a remarkable decrease in the TFEB downregulation–induced upregulation of ANP and β-MHC (Fig. 3*F*). The data suggest that a decrease in GATA4 autophagic degradation contributes to TFEB downregulation–induced cardiomyocyte hypertrophy.

In addition to GATA4, TFs NFAT3 and MEF2 have also been shown to have critical role in the development of cardiac hypertrophy. The enhanced nuclear translocation of NFAT3 and increased MEF2 expression can induce fetal gene expressions and hypertrophic growth of the heart. To test whether TFEB-mediated autophagic flux participates in regulation of these TFs, we examined the influence of TFEB KD on NFAT3 translocation and MEF2 (MEF2A and MEF2B) protein levels. The results show that TFEB KD had no effects on them (Fig. S6), suggesting TFEB KD specifically modulates GATA4 protein content.

Activation of TFEB inhibits cardiomyocyte hypertrophy by encouraging GATA4 autophagic degradation

The aforementioned findings suggest that TFEB presents a potential therapeutic target for the treatment of cardiac hypertrophy. Therefore, we examined the effect of increasing TFEB expression on PE-induced cardiomyocyte hypertrophy. As illustrated in Figure 4, *A* and *B*, the mRNA levels of NPPA and MYH7B and cell-surface area were decreased, indicating that TFEB overexpression largely attenuated the cardiomyocyte hypertrophy. PE resulted in LC3II flux suppression, which was largely attenuated by TFEB overexpression (Fig. 4*C*). The GATA4 accumulation induced by PE was also alleviated by TFEB overexpression (Fig. 4*D*). Furthermore, the protective effect of TFEB overexpression against PE stimulation was weakened by CQ, where ANP and β-MHC expression increased and GATA4 levels accumulated (Fig. 4*E*). The data collectively indicate that TFEB overexpression attenuates PE-induced cardiomyocyte hypertrophy by promoting GATA4 autophagic degradation. Curcumin analog compound C1 is an mTOR-independent activator of TFEB that binds to TFEB to promote its nuclear translocation (49) and may exert a similar therapeutic effect on cardiomyocyte hypertrophy by increasing TFEB expression. As anticipated, PE hindered TFEB nuclear translocation (Fig. 5*A*), and C1 (5 nmol/l, 24 h) promoted TFEB nuclear translocation and attenuated PE-induced cardiomyocyte hypertrophy, as demonstrated by decreased mRNA levels of NPPA and MYH7B (Fig. 5, *B* and *C*). Through the activation of TFEB, C1 alleviated PE-induced autophagic flux inhibition (Fig. 5*D*) and GATA4 accumulation (Fig. 5*E*). In the presence of CQ, the antihypertrophic effect of C1 was weakened, in which ANP and β-MHC expression and GATA4 levels increased (Fig. 5*F*). These data confirm that C1 also attenuates PE-induced cardiomyocyte

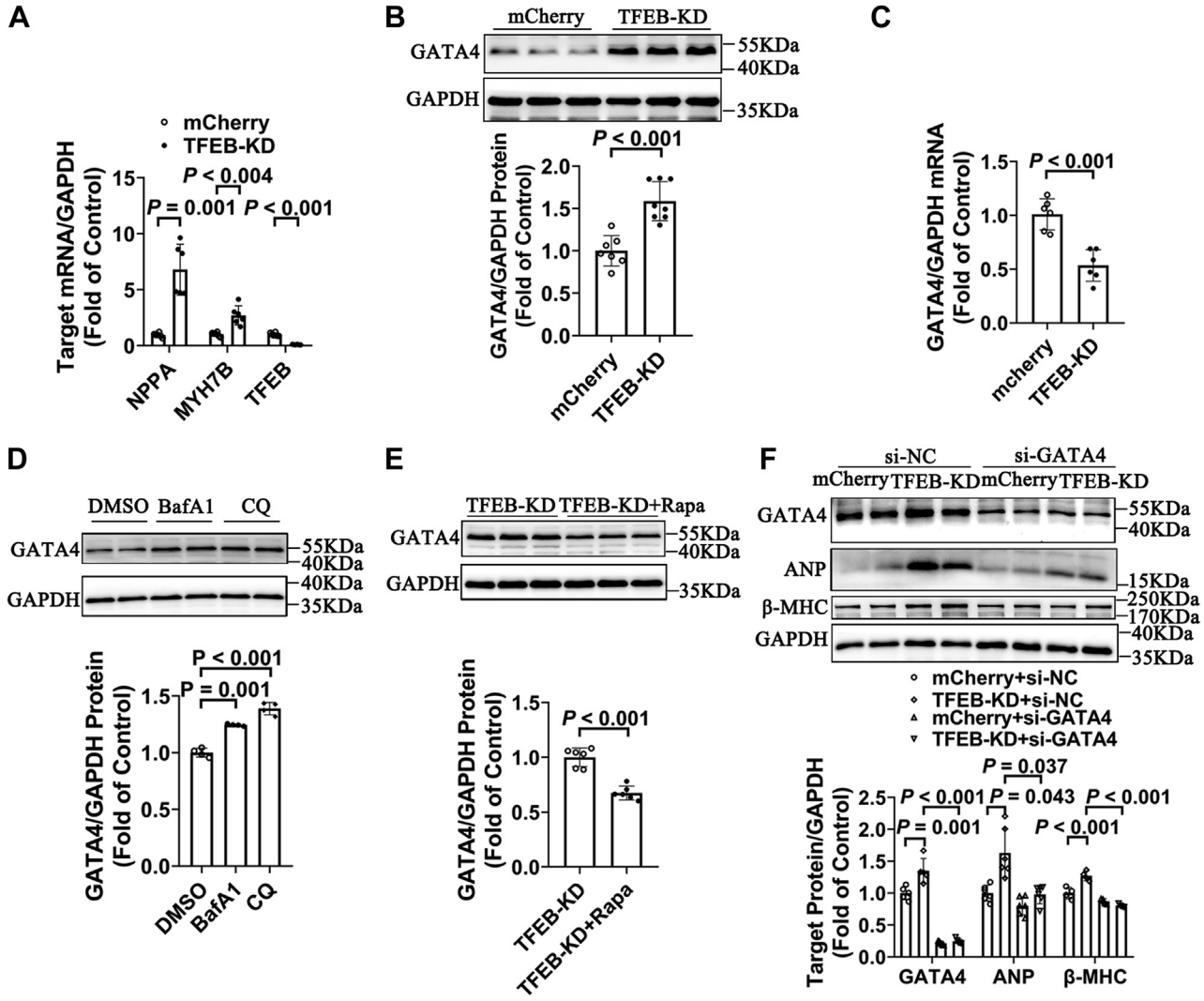

Figure 3. Transcription factor EB (TFEB) downregulation inhibits GATA4 autophagic degradation. *A*, statistics of natriuretic peptide precursor A (NPPA), myosin heavy chain 7B (MYH7B), and TFEB mRNA levels in neonatal rat ventricular myocytes (NRVMs) infected with mCherry control or TFEB-KD (TFEB-knockdown) adenoviruses. n = 6. Data represent mean ± SD from four independent experiments. *B*, representative immunoblot images and statistics of GATA4 protein expression in the two groups. n = 7 to 8. Data represent mean ± SD from four independent experiments. *C*, representative statistics of GATA4 mRNA levels in negative control or TFEB-KD cells. n = 6. Data represent mean ± SD from three independent experiments. *D*, representative immunoblots and statistics of GATA4 protein expression in NRVMs treated with dimethyl sulfoxide (DMSO), bafilomycin A1 (BafA1; 50 nmol/l, 6 h), or chloroquine (CQ; 20 μmol/l, 24 h). n = 4. Data represent mean ± SD from three independent experiments. *E*, representative immunoblots and statistics of GATA4 protein levels in TFEB-KD cells in response to rapamycin (Rapa; 20 μmol/l, 36 h). n = 6. Data represent mean ± SD from three independent experiments. *F*, representative immunoblots and statistics of GATA4, atrial natriuretic peptide (ANP), and myosin heavy chain-β (β-MHC) protein levels in NRVMs of four groups as labeled. n = 4 to 6. Data represent mean ± SD from three independent experiments.

hypertrophy by promoting GATA4 autophagic degradation and may serve as a new drug for the treatment of cardiac hypertrophy.

TFEB overexpression in mouse heart attenuates TAC-induced cardiac hypertrophy

The therapeutic effect of upregulating TFEB on the treatment of cardiac hypertrophy was further examined *in vivo*. We specifically increased cardiac TFEB expression by injecting AAV 9 carrying the cTNT promoter and TFEB gene (TFEB AAV) into mouse tail veins. The control mice received an injection of GFP-AAV. One week after AAV injection, the mice were subjected to TAC or sham surgery for 8 weeks. In the GFP-AAV mice, the left ventricular (LV) posterior wall at systole and diastole was significantly thicker in the mice subjected to TAC compared with sham surgery (Fig. 6, *A* and *B*). The systolic and diastolic LV internal dimensions (LVIDs and LVIDd, respectively) were increased, and the ejection fraction (EF) and fractional shortening (FS) were significantly decreased in TAC compared with sham mice (Fig. 6, *A* and *B*). Congruently, the heart weight/body weight (BW) and lung weight/BW ratios (Fig. 6*C*), as well as NPPA and MYH7B mRNA levels, were dramatically increased in the TAC group (Fig. 6*E*). The images of heart crosssections showed that the gross heart size and myofibril-crossed areas of wheat germ agglutinin (WGA) staining were increased in TAC compared with sham mice (Fig. 6*D*). Furthermore, TAC induced cardiac fibrosis, as Masson's trichrome staining and the semi-quantitative analysis of collagen volume showed that

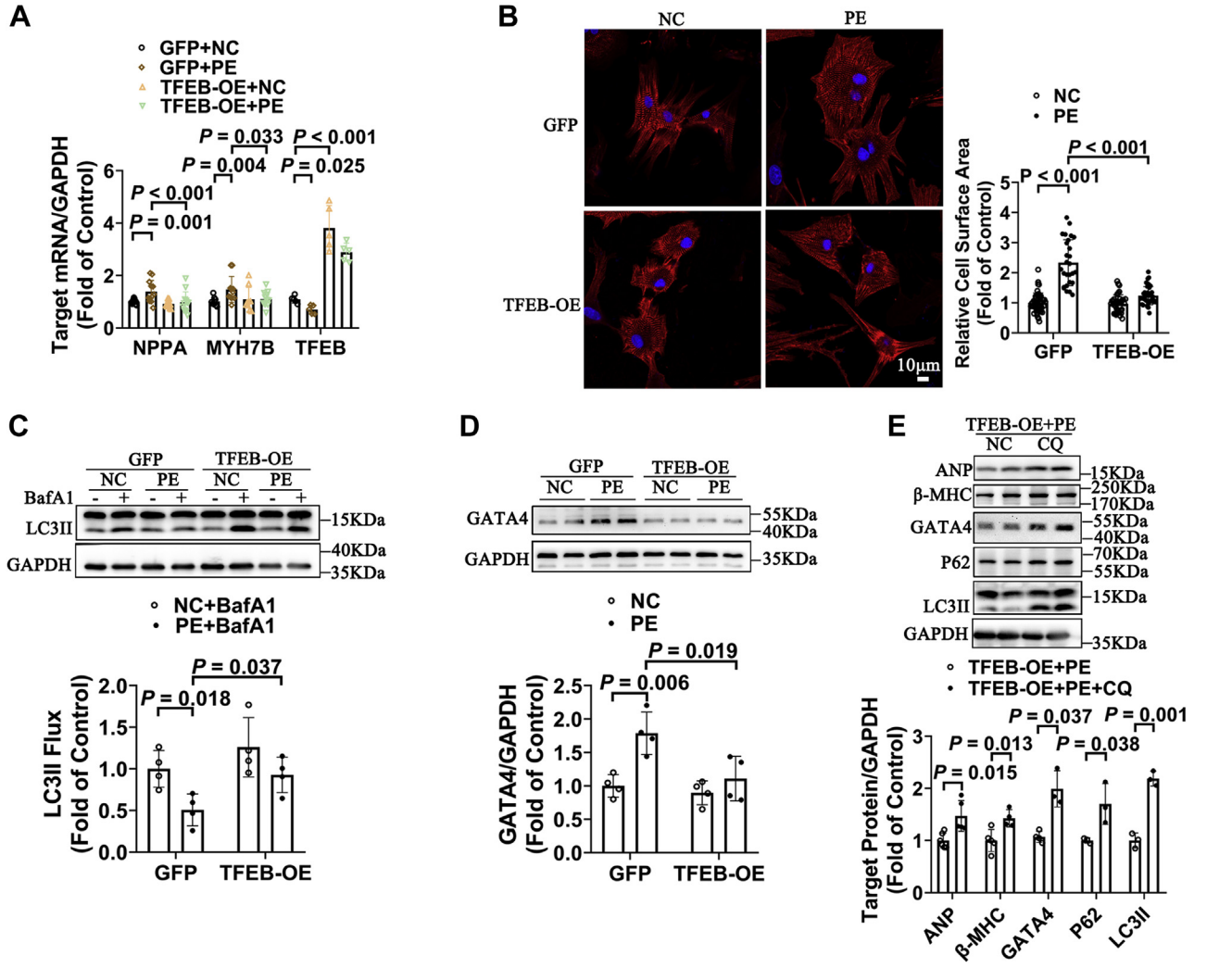

Figure 4. Transcription factor EB (TFEB) overexpression attenuates phenylephrine (PE)-induced hypertrophy by encouraging GATA4 autophagic degradation. *A*, statistics of natriuretic peptide precursor A (NPPA), myosin heavy chain 7B (MYH7B), and TFEB mRNA levels in neonatal rat ventricular myocytes (NRVMs) infected with GFP or TFEB overexpression (OE) lentiviruses with or without PE treatment. n = 5 to 12. Data represent mean ± SD from at least three independent experiments. *B*, representative images and statistics of the cell-surface areas in the four groups. n = 27 to 49 cells from three animals. Data represent mean ± SD from three independent experiments. *C*, representative immunoblots of microtubule-associated protein 1 light chain 3 type II (LC3II) protein levels and statistics of LC3II flux in the labeled groups. The calculation was as described in the Experimental procedures section. n = 4. Data represent mean ± SD from three independent experiments. *D*, representative immunoblots and statistics of GATA4 protein expression in the four groups. n = 4. Data represent mean ± SD from three independent experiments. *E*, representative blots and statistical data of atrial natriuretic peptide (ANP), myosin heavy chain-β (β-MHC), GATA4, P62, and LC3II protein expression in PE (50 μmol/l, 48 h)-treated TFEB-overexpressing NRVMs with or without chloroquine (CQ; 20 μmol/l, 24 h) treatment. n = 3 to 6. Data represent mean ± SD from three independent experiments.

interstitial and perivascular fibrosis had noticeably increased (Fig. 6*G*). The mRNA levels of cardiac fibrosis parameters, including periostin, collagen type III α1, and collagen type I α2, were also significantly higher in the TAC mice (Fig. 6*H*). Along with the structural and functional changes, the protein levels of LC3II and P62 were significantly increased, and more GATA4 accumulated in TAC mouse hearts compared with sham hearts (Fig. 6*F*). Consistent with the blockage of autophagic flux, there was an impairment of mitochondrial function, where PGC1α protein levels and ROS production were significantly decreased in TAC hearts compared with control (Fig. S7, *A* and *B*). Tunnel staining demonstrated that TAC induced cardiomyocyte apoptosis (Fig. S7*C*).

Cardiac TFEB overexpression in mouse heart tissues, which was confirmed by the increase in TFEB mRNA and protein levels (Fig. 6, *E* and *F*), alleviated TAC-induced cardiac hypertrophy, and all hypertrophic changes were markedly reduced 8 weeks post-TAC surgery compared with the TAC mice that received the GFP-AAV injection (Fig. 6, *A*–*H*). In addition, TFEB overexpression attenuated TAC-induced cardiac dysfunction, as the LV EF and FS were significantly increased in TFEB-AAV TAC mice compared with GFP-AAV TAC mice, meanwhile, the heart rate of the two groups was undifferentiated (Fig. 6*B* and Fig. S1). Furthermore, TFEB overexpression relieved the TAC-induced cardiac fibrosis (Fig. 6, *G* and *H*).

Our *in vitro* experiments demonstrated that TFEB overexpression alleviates PE-induced cardiomyocyte hypertrophy by promoting autophagic flux and increasing GATA4 autophagic degradation. TFEB overexpression decreased the TAC-

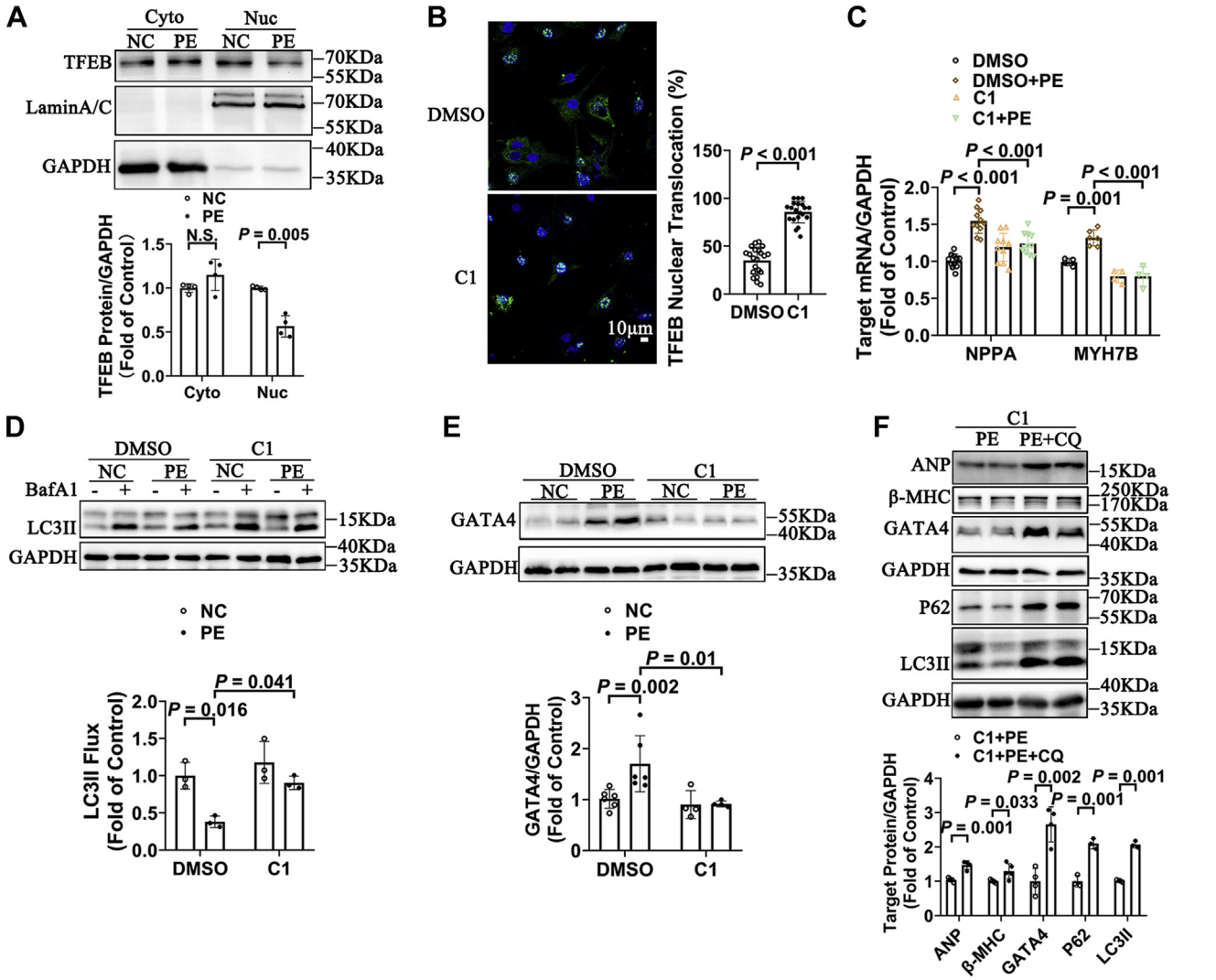

Figure 5. Curcumin analog compound (C1) attenuates phenylephrine (PE)-induced hypertrophy by encouraging GATA4 autophagic degradation. *A*, representative immunoblots and statistics of cytoplasmic (cyto) and nuclear (nuc) transcription factor EB (TFEB) protein levels in neonatal rat ventricular myocytes (NRVMs) treated with or without PE. n = 4. Data represent mean ± SD from three independent experiments. *B*, representative immunofluorescence images and statistics of the TFEB nuclear translocation percentage in NRVMs. n = 20 to 21 cells from three animals. Data represent mean ± SD from three independent experiments. *C*, statistics of natriuretic peptide precursor A (NPPA) and myosin heavy chain 7B (MYH7B) mRNA levels in NRVMs groups as labeled. n = 4 to 11. Data represent mean ± SD from at least three independent experiments. *D*, representative immunoblots of microtubule-associated protein 1 light chain 3 type II (LC3II) protein levels and statistics of LC3II flux in NRVMs treated with dimethyl sulfoxide (DMSO) or C1 (5 μmol/l, 24 h) with or without BafA1 (bafilomycin; 50 nmol/l, 6 h). n = 3. Data represent mean ± SD from three independent experiments. *E*, representative blots and statistical data of GATA4 protein levels in the four groups. n = 4 to 6. Data represent mean ± SD from three independent experiments. *F*, representative immunoblots and statistics of atrial natriuretic peptide (ANP), myosin heavy chain-β (β-MHC), GATA4, P62, and LC3II protein levels in NRVMs treated with PE and C1 with or without CQ (20 μmol/l, 24 h) treatment. n = 3 to 5. Data represent mean ± SD from at least three independent experiments. N.S., not significant.

induced upregulation of P62 and GATA4 protein levels (Fig. 6*F*). The impaired mitochondrial activities were restored by TFEB overexpression in TAC mice, where PGC1 expression was increased and ROS production and cardiomyocyte apoptosis were decreased (Fig. S7, *A*–*C*), confirming the protective effects of TFEB on mitochondrial function *in vivo*.

Discussion

Here, we report, to our knowledge, the first evidence for the critical role of TFEB in the development of pathological cardiac hypertrophy. Under stress by catecholamine stimulation (PE) and PO (TAC), TFEB expression in the heart is decreased, leading to autophagic flux blockage and ALP insufficiency. TFEB insufficiency, particularly, impairs the autophagic degradation pathway of GATA4, and an accumulation of GATA4 increases prohypertrophic gene expression, promoting the pathological remodeling of the heart. Activation of TFEB, genetically or pharmacologically, restores autophagic flux and GATA4 degradation, providing a promising therapeutic strategy for the treatment of pathological cardiac hypertrophy.

Decreased TFEB expression contributes to ALP insufficiency and pathological cardiac hypertrophy

Although current opinion states that ALP insufficiency occurs in cardiac hypertrophy (12–17), direct evidence of ALP

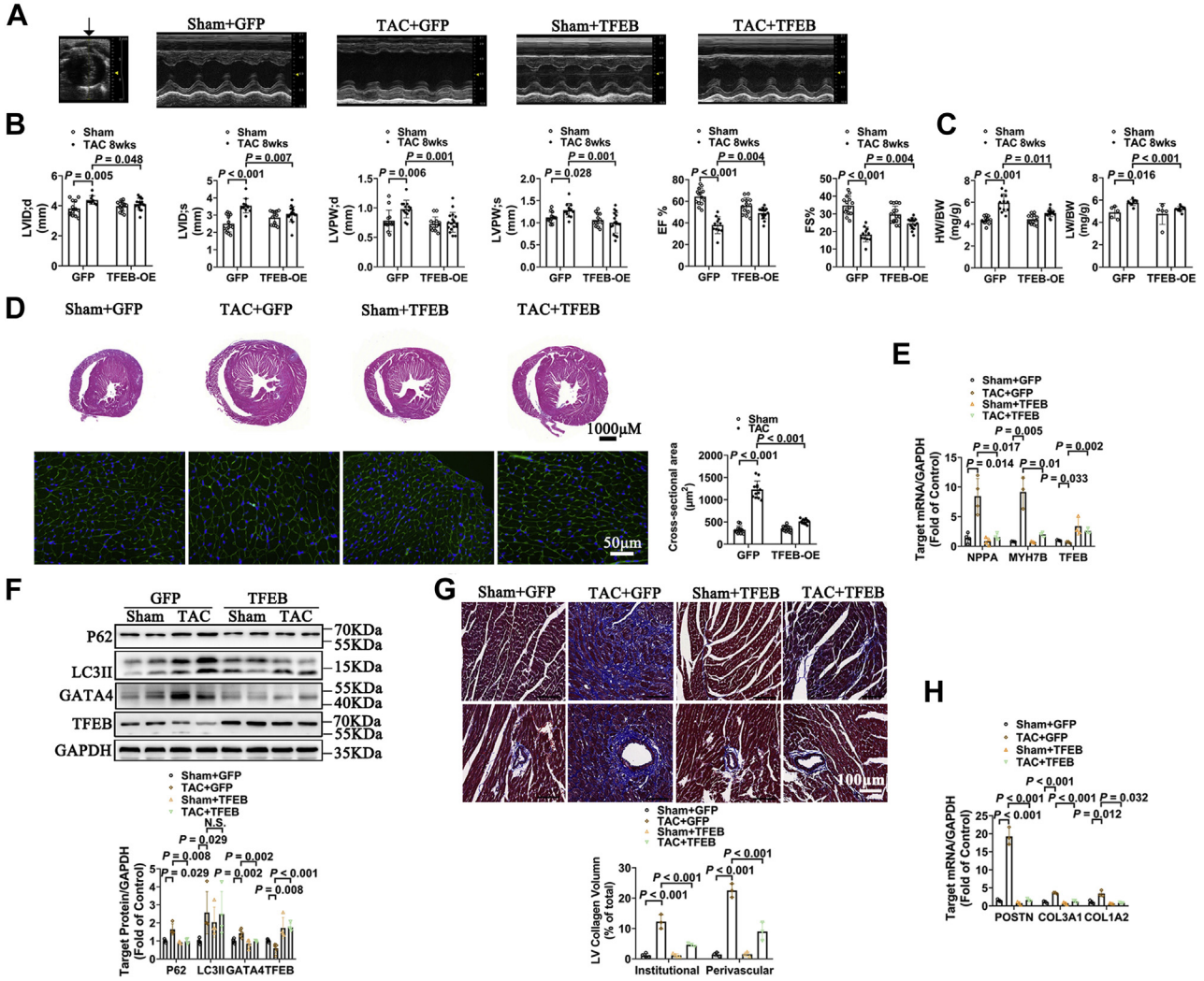

Figure 6. Transcription factor EB (TFEB) overexpression in mouse heart attenuates transverse aortic constriction (TAC)–induced cardiac hypertrophy. *A*, representative M-mode tracing from the echocardiography of GFP and TFEB overexpression mice 8 weeks after sham or TAC operation. *B*, systolic left ventricular internal dimension (LVIDs) and diastolic left ventricular internal dimension (LVIDd), thicknesses of the left ventricular posterior wall at systole (LVPWs) and diastole (LVPWd), and left ventricular ejection fraction (EF) and fraction shortening (FS). n = 10 to 17. Data represent mean ± SD from two independent experiments. *C*, statistics of heart weight/body weight (HW/BW) ratio and wet lung weight/body weight (LW/BW) ratio. n = 5 to 12. Data represent mean ± SD from two independent experiments. *D*, representative images of hematoxylin and eosin staining of transverse sections of hearts, and representative images and statistics of wheat germ agglutinin staining of hearts from the four mouse groups. n = 12 fields from three mice per group. Data represent mean ± SD from one independent experiment. *E*, statistics of natriuretic peptide precursor A (NPPA), myosin heavy chain 7B (MYH7B), and transcription factor EB (TFEB) mRNA levels in mouse hearts from the labeled four groups. n = 3 to 4. Data represent mean ± SD from one independent experiment. *F*, representative immunoblots and statistics of P62, microtubule-associated protein 1 light chain 3 type II (LC3 II), GATA4, and TFEB protein levels in the mouse hearts. n = 4 to 5. Data represent mean ± SD from one independent experiment. *G*, representative images and statistics of Masson's trichrome staining of hearts. n = 3 to 4 fields from 3 to 4 animals. The statistics was from the panoramic scanning pictures. Data represent mean ± SD from one independent experiment. *H*, statistics of periostin (POSTN), collagen type III, alpha 1 (COL3A1), and collagen type I, alpha 2 (COL1A2) mRNA levels in mouse hearts from the four labeled groups. n = 3. Data represent mean ± SD from one independent experiment.

insufficiency promoting pathological cardiac remodeling is still lacking, and the mechanisms are unknown. Therefore, strategies to improve ALP in pathological cardiac hypertrophy are often nonspecific. The best way to manipulate autophagy to exert antihypertrophic remodeling is of clinical significance and urgently needs to be addressed.

TFEB has been shown to play protective roles in cardiac damages including myocardial ischemia-reperfusion injury, doxorubicin, and proteotoxicity-induced cardiac toxicity, monoamine oxidase-A–induced HF, and missense variant in Rag GTPase protein C–induced syndromic dilated cardiomyopathy *via* autophagy-dependent or autophagy-independent pathways. Whether TFEB regulates ALP in cardiac hypertrophy and the regulation is beneficial or detrimental to the heart in the context of cardiac pathological remodeling remain unknown, as one study reported that cardiac-specific overexpression of TFEB induces pathological cardiac hypertrophy and lethal cardiomyopathy using a doxycycline-inducible Tet-off mouse model.

This study was the first to demonstrate the critical role of TFEB downregulation in ALP insufficiency in cardiomyocytes, and we showed that knocking down TFEB increased LC3II and P62 protein levels and decreased autophagic flux (LC3II flux decreased and autophagolysosome levels decreased). We further

established a causal relationship between TFEB downregulation–induced ALP insufficiency and the pathogenesis of cardiac hypertrophy: knocking down TFEB induced the hypertrophic growth of NRVMs, and promoting autophagy flux with rapamycin or by overexpression ATG7 attenuated TFEB KD-induced cardiomyocyte hypertrophy. Therefore, our study identified TFEB as a possible target for manipulation to effectively address ALP insufficiency in the treatment of cardiac hypertrophy.

In contrast to the remarkably detrimental effect of TFEB overexpression on the hearts in the conditional cardiac-specific TFEB transgenic mice (37), we did not observe significant damage of mouse hearts with AAV9-mediated TFEB overexpression. In the transgenic mouse model, there is an approximately eightfold increase in TFEB protein expression, whereas there is only a twofold increase in TFEB protein in TFEB-overexpressed animals in our study. The moderate increase in TFEB has moderate effect on autophagy and cardiac function as found in our study, whereas exaggerated autophagy and perhaps autophagy-independent noncanonical effect of TFEB induces heart damage as observed in the transgenic mice. The differential outcome in the hearts with TFEB overexpression between the two studies suggests that the expression levels of TFEB should be carefully manipulated to prevent insufficient or exaggerated autophagy-induced damage to the heart.

TFEB downregulation induces GATA4 autophagic blockage, contributing to the pathogenesis of cardiac hypertrophy

The pathogenesis of PO-induced cardiac hypertrophy is tightly related to the activation of several TFs, including GATA4, NFAT, and MEF2 (47, 50). Our results showed that TFEB KD leads to an accumulation of GATA4, a TF that plays an essential role in the development of cardiac hypertrophy by regulating the expression of several fetal genes, that is, NPPA, NPPB, and MYH7B, which promote cardiomyocyte growth (46, 47, 51, 52).

We generated several lines of evidence indicating the causal relationship between GATA4 accumulation and TFEB-induced cardiac hypertrophy. First, we observed decreased TFEB and increased GATA4 protein levels in both *in vitro* PE-stimulated cardiomyocyte hypertrophy and TAC-induced mouse cardiac hypertrophy models. Second, TFEB KD markedly increased the mRNA levels of the fetal genes NPPA and MYH7B, and the transcription of these genes was upregulated by GATA4. Third, knocking down GATA4 expression largely inhibited cardiomyocyte hypertrophy upon TFEB KD in NRVMs. Therefore, GATA4 accumulation contributes to TFEB-induced cardiac hypertrophy.

Of note, TFEB overexpression or C1 treatment increased autophagic flux without changing basal GATA4 protein level (Fig. 4*D*). The protein level of GATA4 is determined by the balance of GATA4 protein stability and protein synthesis, while autophagy is just one mechanism that directly regulates the protein stability and may indirectly regulate protein synthesis. Under normal condition, the balance can be well maintained when there is a moderate increase (by 1.25-fold by TFEB overexpression and 1.17-fold by C1 treatment) in autophagy flux. GATA4 synthesis may be increased, and/or proteasome-mediated GATA4 degradation may be decreased to compensate for the enhanced autophagy-induced GATA4 degradation. This study is limited by that we have no data to explain why increasing autophagy flux under normal condition had no effect on GATA4 protein level, while restoring the impaired autophagy flux under hypertrophic conditions reduced GATA4 accumulation. We propose it is attributed to the difference of the complicated regulation system of GATA4 protein under normal and pathological conditions.

Interestingly, under differential pathological conditions, TFEB-mediated autophagy is likely to have specific roles in regulating signaling pathways relating to the disease. For example, in Cry ABR 120G-induced cardiac proteinopathy, TFEB overexpression can upregulate HSPB8 to restore normal desmin location (39). While in doxorubicin-induced cardiotoxicity, TFEB offered protection for dihydrotanshinone I against doxorubicin-induced cardiotoxicity by downregulating phosphorylation of inhibitor of κb kinase α/β and NF-κB (53). TFEB overexpression has also been shown to attenuate autophagosome buildup and mitochondrial fission in monoamine oxidase-A–induced HF (54). In this study, we reported TFEB-mediated GATA4 autophagic degradation, which promotes pathological cardiac hypertrophy.

To explore the mechanism of TFEB-induced GATA4 accumulation, we examined the mRNA levels of GATA4 and found them to be decreased, contrary to the change in GATA4 protein levels. This indicates that TFEB may induce GATA4 accumulation through post-transcriptional modification. Interestingly, we found a novel autophagy-mediated protein degradation pathway controlling GATA4 protein levels in neonatal cardiomyocytes, as GATA4 protein stability was increased when autophagic flux was blocked by BafA1 and CQ. This regulation, at least partially, accounts for TFEB-induced GATA4 accumulation. Supporting evidence included the decrease in GATA4 autophagic degradation by blocking ALP flux via TFEB downregulation, and the alleviation of TFEB KD induced GATA4 accumulation by rapamycin and ATG7 enhancement of ALP.

A recent study reported that GATA4 was degraded by P62-mediated selective autophagy in human senescent lung cells (48). P62 was shown to be a receptor that interacts with GATA4 and mediates the lysosomal degradation of GATA4. In this study, we found that TFEB KD increased P62 protein levels *via* autophagic flux blockage. Nevertheless, we did not observe an interaction between P62 and GATA4 in the co-immunoprecipitation (IP) assay (Fig. S2), suggesting that the autophagic degradation of GATA4 in cardiomyocytes may not require P62 as an adaptor. Whether TFEB-mediated bulk autophagy is responsible for GATA4 degradation or a special adaptor is needed for GATA4 autophagic degradation in cardiomyocytes awaits future study.

Activation of TFEB protects against PO-induced cardiac hypertrophy

We explored the therapeutic potential of TFEB activation in the treatment of PO-induced cardiac hypertrophy. We first

overexpressed TFEB in cardiomyocytes and mouse hearts, which had a therapeutic effect on PE-induced cardiomyocyte hypertrophy and TAC-induced cardiac hypertrophy, resulting in significantly decreased ANP and β-MHC expression and cell size. These therapeutic effects can be attributed to the TFEB promotion of ALP flux and GATA4 degradation, since blocking autophagy flux with CQ weakened the protective effect of TFEB against cardiac hypertrophy and GATA4 accumulation.

The preventative effect of manipulating TFEB expression on the development of cardiac hypertrophy and HF is encouraging. However, this study is limited by not exploring whether targeting TFEB after the onset of hypertrophic stimulation (post-TAC) still has a therapeutic effect on cardiac pathological remodeling and HF, which would be more instructive for potential clinical translation. There are controversies about the temporal specific roles of autophagy in the progression of HF. In this study, we also examined the time-dependent changes of TFEB expression and autophagy flux at the compensatory stage of cardiac hypertrophy and found that these parameters did not significantly change 3 days post-TAC but remarkably decreased 7 days post-TAC (Fig. S5*A*) and remained at the low levels 14 days post-TAC (Fig. S5, *B* and *C*). Therefore, activation of TFEB is recommended to be applied at the early stage of cardiac hypertrophy to reverse the pathological remodeling, which warrants future study.

Given the possible side effects of adenovirus or AAV transfection, we further explored the pharmacological activation of TFEB using the curcumin analog compound, C1, an mTOR-independent activator of TFEB that specially binds to TFEB at the N terminus to promote TFEB nuclear translocation. Similar to the effect of TFEB overexpression, C1 protected against PE-induced hypertrophy by restoring ALP flux and GATA4 autophagic degradation. Further, we found that TAC decreased the nuclear translocation of TFEB (Fig. S3), suggesting the efficiency of C1 on TAC-induced cardiac hypertrophy. C1 has previously been shown to be effective in the treatment of pulmonary fibrosis (55). This study implicated C1 as a therapeutic candidate for the treatment of cardiac hypertrophy.

In addition to hypertrophic growth, cardiac fibrosis is another prominent outcome from the pathological remodeling of hypertensive heart disease. Because cardiac hypertrophy and fibrosis are mutually promoted (56), a strategy to target both hypertrophy and fibrosis should have better clinical efficacy. Existing reports indicate that improving autophagic flux can attenuate cardiac fibrosis (57–61), and TFEB is known to protect against lung fibrosis (30, 55). Our study demonstrated that cardiac-specific TFEB overexpression has a pronounced therapeutic effect on TAC-induced cardiac fibrosis. How TFEB in cardiomyocytes exerts the antifibrosis effect and whether the activation of TFEB in cardiac fibroblasts has a similar effect in the context of PO-induced cardiac hypertrophy have not been explored and deserve further investigation.

Experimental procedures

Animals

C57BL/6 wildtype male mice were purchased from the Animal Center of Southern Medical University. The mice were kept caged with a 12-h light/dark cycle and allowed free access to food and water. All animal protocols were approved by the Shenzhen University Institutional Care and Ethical Committee and complied with Guidelines for the Care and Use of Laboratory Animals published by the National Academy Press (National Institutes of Health [NIH]; publication no. 85-23, revised 1996). For isolation of the heart, mice were euthanized by an intraperitoneal injection of sodium pentobarbital with the dosage of 150 mg/kg.

Human heart samples

Human studies were performed in line with the Declaration of Helsinki. Human heart samples were procured according to protocols approved by the Institutional Review Boards on Human Subjects of Zhongshan People's Hospital, China. Healthy donator and patients with cardiomyopathy have provided informed consent for the collection of tissues. Heart tissues were obtained and flash frozen at the time of heart transplantation and stored in liquid nitrogen until use.

AAV injection and TAC

For TFEB overexpression *in vivo*, the coding regions of TFEB (NM_011549.3) were cloned and then delivered into the recombinant AAV9 plasmid with the promoter for cTnT. The AAV construction was finished at OBiO Technology Company. AAV was injected *via* the tail vein, and the method was proceeded as described (33).

C57BL/6 male (10–11 weeks, 23–27 g) mice were randomly divided into four groups: sham and TAC with or without TFEB overexpression. The TAC surgery was operated as previously described (37). Briefly, mice were anesthetized with 50 mg/kg pentobarbital sodium, and a small incision was made at the second intercostal space to expose the aortic arch. The transverse aorta was isolated and constricted with a 7-0 nylon suture tied against a 27-gauge needle. The needle was removed to yield a constriction of 0.4 mm in diameter thereafter. The suture was not tied in the sham surgery. AAV-TFEB/GFP was injected *via* the tail vein at a dose of 1×10^{11} virus genome/per mouse 1 week after TAC operation.

NRVM culture

NRVMs were used for all the experiments *in vitro* in this study, and they were isolated from 1- to 2-day-old Sprague–Dawley rats. As reported previously (34), tissues were mechanically crushed in cold PBS and then transferred into 0.125% trypsin (in PBS). Digestion, for one cycle, involved a 15-min incubation at 37 °C and centrifugation of the suspension, then resuspending precipitation in Dulbecco's modified Eagle's medium (Life Technologies) with 10% fetal calf serum (Life Technologies) and penicillin (100 U/ml)/streptomycin (100 μg/ml) (Life Technologies). Four cycles later, the fibroblasts were removed from the resuspension by differential plating at 37 °C in 5% CO_2 for 90 min. NRVMs were distributed into corresponding dishes, and the media

were renewed after 24-h incubation with 100 μM 5-bromodeoxyuridine (Sigma–Aldrich).

Virus infection

To suppress the expression of TFEB in NRVMs, we used an mCherry-tagged recombinant adenovirus encoding TFEB-targeting short hairpin RNA (sh-TFEB; OBiO). The target sequence for rat TFEB was "GCTACACATCAGCTCCAAT." To overexpress TFEB in NRVMs, we used a GFP-tagged recombinant adenovirus encoding full-length TFEB (Ad-TFEB; OBiO). The null adenoviral vector and the recombinant adenovirus expressing GFP was used as the control for TFEB KD and overexpression experiments.

To measure autophagic flux, we used microtubule-associated protein 1 light chain 3 type II B tandemly tagged with an acid-resistant monomeric RFP and acid-sensitive GFP (mRFP-GFP-LC3B) adenovirus (HanBio) to detect the formation of autophagosomes (RFP^+ GFP^+ signal) and autolysosomes (RFP^+ GFP^- signal). Images were acquired on a fluorescence microscope (Zeiss), and the number of punctas were counted using ImageJ software (the NIH).

NRVMs were infected (MOI = 30) with adenoviruses for 16 h and were harvested or fixed until the end of the sequential treatments.

The LC3II flux assay

The LC3II flux refers to the net amount of LC3II accumulated by BafA1-induced lysosomal inhibition, and it was calculated by subtracting the GAPDH-normalized LC3II levels of BafA1-treated samples from the GAPDH-normalized LC3II levels of the vehicle control samples.

siRNA transfection

NRVMs were cultured in 35-mm confocal dishes for 24 h, then transfected with control random siRNA or rat TFEB and GATA4-targeted SiRNA (si-NC, si-TFEB, and si-GATA4; designed and synthesized by Shanghai Biotend Biotechnology) using Lipofectamine RNAimax (Invitrogen) in accordance with the manufacturer's instructions. The TFEB siRNA sequences were as follows: sense strand "GCGAGAGCUAACAGAUGCUdTdT" and antisense strand "AGCAUCUGUUAGCUCUCGCdTdT." The GATA4 siRNA sequences were as follows: sense strand "GCUGCAGCCUACAGCAGUAdTdT" and antisense strand "UACUGCUGUAGGCUGCAGCdTdT." After culture for 24 h, cardiomyocytes were transfected with si-NC or si-TFEB and si-GATA4 (50 nmol) for 72 h.

Quantitative real-time PCR

Tissues and NRVMs were lysed in TRI-zol reagent, and mRNA extraction was implemented following the manufacturer's instructions. Reverse transcription of 1 μg RNA was implemented using the ReverTra Ace qPCR RT Master Mix with gDNA Remover kit (TOYOBO). RT-PCR with Real-Time PCR Master Mix (TOYOBO) was performed using Step One plus. Operations in reverse transcription and real-time PCR were implemented in accordance with corresponding manuals of TOYOBO. The primers for quantitative RT-PCR in this study are listed in Table S2. The mRNA levels were normalized to GAPDH by the $2^{-\triangle\triangle CT}$ method.

Western blot

Tissues and cells were lysed in radioimmunoprecipitation assay cell lysis buffer (Solarbio) supplemented with protease and phosphatase cocktail inhibitors (Roche) to obtain total protein. Protein concentration was determined using a protein quantitative assay kit (Pierce). Nuclear protein extraction was performed using the Nuclear and Cytoplasmic Protein Extraction kit (Beyotime Biotechnology) in accordance with the manufacturer's instructions. Protein extracts were resolved by SDS-PAGE and transferred to polyvinylidene fluoride membranes (Millipore). After blocking with 5% nonfat milk in Tris-buffered saline containing 0.1% Tween-20, membranes were incubated with respective antibodies (summarized in Table S1) at 4 °C overnight. After washing, the membranes were incubated with horseradish peroxidase–conjugated antimouse or anti-rabbit immunoglobulin G (CST). The relative densitometry of bands was measured by ImageJ software (NIH) and then normalized to their respective loading control.

Immunofluorescence

NRVMs were fixed by 4% paraformaldehyde in PBS for 15 min and permeabilized with 0.1% Triton X-100 in PBS for 15 min and then blocked with 3% bovine serum albumin (Solarbio) in PBS for 1 h. NRVMs were incubated with the target primary antibody at a dilution of 1:200 overnight. After rigorous washing, the secondary antibody conjugated with Alexa Fluor 633 nm (1:200; Invitrogen) or Alexa Fluor 488 nm (1:200; Invitrogen) was added for 2 h at room temperature. We used 4′6-diamidino-2-phenylindole to stain the nuclei. Images were acquired on a fluorescence microscope (Zeiss), and all images were obtained under the same conditions.

Cell surface area measurements

The surface area of a single myocyte was measured using the Image Pro Plus Data Analysis Program (Media Cybernetics). Cells in each group were randomly selected from three independent experiments, and only cells lying fully within the visual field were quantified.

Echocardiography assay

M mode echocardiography was obtained using a Vevo 2100 Ultrasound System (Visual Sonics) equipped with a high-frequency (30 Hz) linear array transducer. M-mode echocardiography was performed at 8 weeks after TAC surgery, and mice were anesthetized with a mixture of isoflurane (1.5%) and oxygen (2 l/min). For two-dimensional guided M-mode echocardiography, the heart image was captured in the two-dimensional mode in the parasternal short-axis view, and the following parameters were

measured: LV internal dimensions at both diastole and systole (LVIDd and LVIDs), LV posterior wall dimensions at both diastole and systole (LV posterior wall at diastole and LV posterior wall at systole), percentage of LV EF and LV FS. Measurements were made from leading edge to leading edge according to the American Society of Echocardiography guidelines. The percentage EF (%) was calculated as $[(LVIDd^2 - LVIDs^2)/LVIDd^2] \times 100$, and the LV FS (%) was calculated as $[(LVIDd - LVIDs)/LVIDd] \times 100$.

Morphology and histology

Mice were anesthetized and weighed to obtain the BW. The heart was rapidly excised after perfusion with PBS, and the residual liquid was absorbed by filter paper. Then the heart weight and lung weight were measured. Heart tissues were cross-sectioned, and the sections were fixed in 3.7 to 4% paraformaldehyde and embedded with paraffin. Next, the paraffin-embedded apex was sectioned at 5-μm intervals and stained with hematoxylin and eosin, Masson's trichrome (Sigma–Aldrich), and WGA (Invitrogen) stains according to the manufacturer's instructions. Myofibril-crossed areas were calculated for the WGA-stained images obtained on a fluorescence microscope (Zeiss) using ImageJ software.

IP

Cells were lysed with IP lysis buffer (Thermo Fisher Scientific) supplemented with protease inhibitor cocktail (Roche) at 4 °C. After being sonicated and centrifuged at 12,000*g* for 15 min, the lysates were precleared and incubated with the indicated primary antibodies overnight at 4 °C and then incubated with protein A/G magnetic beads (Thermo Fisher Scientific) for 2 h in the room temperature. The beads were then washed with washing buffer for five times, and then the samples were harvested for Western blot.

Statistical analyses

The "n" in the figure legend refers to the number of data points. And, the data points are equal to biological replicates, and technical replicate of each sample is one. Differences between two groups were evaluated by unpaired Student's *t* tests and between multiple groups by one-way ANOVA with Bonferroni correction. All statistical analyses were performed using the SPSS software, version 22.0 (IBM). In all cases, $p < 0.05$ was considered statistically significant.

Data availability

The data in this study are available from the author Rui Song (songrui8928@163.com) on reasonable request.

Supporting information—This article contains supporting information.

Acknowledgments—The authors thank Dr Jessica Tamanini (Shenzhen University Health Science Center, China and ETediting, United Kingdom) for editing this article before submission. This work was supported by grants from the National Natural Science Foundation of China (grant no.: 31671179, 81970250, and 81870274), Shenzhen Key Laboratory of Metabolism and Cardiovascular Homeostasis (grant no.: ZDSYS20190902092903237), and Basic Research Foundation of Shenzhen (grant no.: JCYJ20180508152222104).

Author contributions—L. L. Y. and J. L. conceptualization; R. S., H. L., L. F., W. C., and Y. L. methodology; R. S., H. L., L. F., W. C., and Y. L. software; L. L. Y. and J. L. validation; R. S., H. L., L. F., W. C., and Y. L. investigation; R. S. and H. L. data curation; R. S. writing–original draft; J. L. writing–review and editing; W. C. and Y. L. visualization; L. L. Y. and J. L. supervision; R. S., H. L., L. F., L. L. Y., and J. L. project administration; L. L. Y. and J. L. funding acquisition.

Conflict of interest—The authors declare that they have no conflicts of interest with the contents of this article.

Abbreviations—The abbreviations used are: β-MHC, myosin heavy chain-β; AAV, adeno-associated virus; ALP, autophagosome–lysosome pathway; ANP, atrial natriuretic peptide; ATG7, autophagy-related protein 7; BafA1, bafilomycin A1; BW, body weight; CQ, chloroquine; EF, ejection fraction; FS, fractional shortening; HF, heart failure; IP, immunoprecipitation; KD, knockdown; LC3, light chain 3; LV, left ventricular; LVIDd, diastolic LV internal dimension; LVIDs, systolic LV internal dimension; MOI, multiplicity of infection; mTORC1, mechanistic target of rapamycin kinase complex 1; NIH, the National Institutes of Health; MYH7B, myosin heavy chain 7B; NPPA, natriuretic peptide precursor A; NPPB, natriuretic peptide precursor B; NRVM, neonatal rat ventricular myocyte; PE, phenylephrine; PGC1α, peroxisome proliferator–activated receptor-gamma coactivator-1α; PO, pressure overload; RFP, red fluorescent protein; TAC, transverse aortic constriction; TF, transcription factor; TFEB, transcription factor EB; WGA, wheat germ agglutinin.

References

1. Wang, X., and Robbins, J. (2014) Proteasomal and lysosomal protein degradation and heart disease. *J. Mol. Cell. Cardiol.* **71**, 16–24
2. Zhang, K. (2018) "NO" to autophagy: Fat does the trick for diabetes. *Diabetes* **67**, 180–181
3. Toledo, M., Batista-Gonzalez, A., Merheb, E., Aoun, M. L., Tarabra, E., Feng, D., Sarparanta, J., Merlo, P., Botre, F., Schwartz, G. J., Pessin, J. E., and Singh, R. (2018) Autophagy regulates the liver clock and glucose metabolism by degrading CRY1. *Cell Metab.* **28**, 268–281
4. Scrivo, A., Bourdenx, M., Pampliega, O., and Cuervo, A. M. (2018) Selective autophagy as a potential therapeutic target for neurodegenerative disorders. *Lancet Neurol.* **17**, 802–815
5. Harris, H., and Rubinsztein, D. C. (2011) Control of autophagy as a therapy for neurodegenerative disease. *Nat. Rev. Neurol.* **8**, 108–117
6. Maejima, Y., Chen, Y., Isobe, M., Gustafsson, A. B., Kitsis, R. N., and Sadoshima, J. (2015) Recent progress in research on molecular mechanisms of autophagy in the heart. *Am. J. Physiol. Heart Circ. Physiol.* **308**, H259–H268
7. Schiattarella, G. G., and Hill, J. A. (2016) Therapeutic targeting of autophagy in cardiovascular disease. *J. Mol. Cell. Cardiol.* **95**, 86–93
8. Kustermann, M., Manta, L., Paone, C., Kustermann, J., Lausser, L., Wiesner, C., Eichinger, L., Clemen, C. S., Schroder, R., Kestler, H. A., Sandri, M., Rottbauer, W., and Just, S. (2018) Loss of the novel Vcp (valosin containing protein) interactor Washc4 interferes with autophagy-mediated proteostasis in striated muscle and leads to myopathy *in vivo*. *Autophagy* **14**, 1911–1927

9. Mozaffarian, D., Benjamin, E. J., Go, A. S., Arnett, D. K., Blaha, M. J., Cushman, M., Das, S. R., de Ferranti, S., Despres, J. P., Fullerton, H. J., Howard, V. J., Huffman, M. D., Isasi, C. R., Jimenez, M. C., Judd, S. E., *et al.* (2016) Heart Disease and Stroke Statistics-2016 update: A report from the American Heart Association. *Circulation* **133**, e38–e360
10. Ponikowski, P., Anker, S. D., AlHabib, K. F., Cowie, M. R., Force, T. L., Hu, S., Jaarsma, T., Krum, H., Rastogi, V., Rohde, L. E., Samal, U. C., Shimokawa, H., Budi, S. B., Sliwa, K., and Filippatos, G. (2014) Heart failure: Preventing disease and death worldwide. *ESC Heart Fail.* **1**, 4–25
11. Frey, N., Katus, H. A., Olson, E. N., and Hill, J. A. (2004) Hypertrophy of the heart: A new therapeutic target? *Circulation* **109**, 1580–1589
12. Qin, Q., Qu, C., Niu, T., Zang, H., Qi, L., Lyu, L., Wang, X., Nagarkatti, M., Nagarkatti, P., Janicki, J. S., Wang, X. L., and Cui, T. (2016) Nrf2-mediated cardiac maladaptive remodeling and dysfunction in a setting of autophagy insufficiency. *Hypertension* **67**, 107–117
13. Shirakabe, A., Zhai, P., Ikeda, Y., Saito, T., Maejima, Y., Hsu, C. P., Nomura, M., Egashira, K., Levine, B., and Sadoshima, J. (2016) Drp1-dependent mitochondrial autophagy plays a protective role against pressure overload-induced mitochondrial dysfunction and heart failure. *Circulation* **133**, 1249–1263
14. Li, M. H., Zhang, Y. J., Yu, Y. H., Yang, S. H., Iqbal, J., Mi, Q. Y., Li, B., Wang, Z. M., Mao, W. X., Xie, H. G., and Chen, S. L. (2014) Berberine improves pressure overload-induced cardiac hypertrophy and dysfunction through enhanced autophagy. *Eur. J. Pharmacol.* **728**, 67–76
15. Matsumura, N., Robertson, I. M., Hamza, S. M., Soltys, C. M., Sung, M. M., Masson, G., Beker, D. L., and Dyck, J. R. (2017) A novel complex I inhibitor protects against hypertension-induced left ventricular hypertrophy. *Am. J. Physiol. Heart Circ. Physiol.* **312**, H561–H570
16. Weng, L. Q., Zhang, W. B., Ye, Y., Yin, P. P., Yuan, J., Wang, X. X., Kang, L., Jiang, S. S., You, J. Y., Wu, J., Gong, H., Ge, J. B., and Zou, Y. Z. (2014) Aliskiren ameliorates pressure overload-induced heart hypertrophy and fibrosis in mice. *Acta Pharmacol. Sin.* **35**, 1005–1014
17. Li, Y., Chen, C., Yao, F., Su, Q., Liu, D., Xue, R., Dai, G., Fang, R., Zeng, J., Chen, Y., Huang, H., Ma, Y., Li, W., Zhang, L., Liu, C., *et al.* (2014) AMPK inhibits cardiac hypertrophy by promoting autophagy via mTORC1. *Arch. Biochem. Biophys.* **558**, 79–86
18. Zhu, H., Tannous, P., Johnstone, J. L., Kong, Y., Shelton, J. M., Richardson, J. A., Le, V., Levine, B., Rothermel, B. A., and Hill, J. A. (2007) Cardiac autophagy is a maladaptive response to hemodynamic stress. *J. Clin. Invest.* **117**, 1782–1793
19. Wang, X., and Cui, T. (2017) Autophagy modulation: A potential therapeutic approach in cardiac hypertrophy. *Am. J. Physiol. Heart Circ. Physiol.* **313**, H304–H319
20. Pan, W., Zhong, Y., Cheng, C., Liu, B., Wang, L., Li, A., Xiong, L., and Liu, S. (2013) MiR-30-regulated autophagy mediates angiotensin II-induced myocardial hypertrophy. *PLoS One* **8**, e53950
21. Yin, X., Peng, C., Ning, W., Li, C., Ren, Z., Zhang, J., Gao, H., and Zhao, K. (2013) miR-30a downregulation aggravates pressure overload-induced cardiomyocyte hypertrophy. *Mol. Cell. Biochem.* **379**, 1–6
22. Napolitano, G., and Ballabio, A. (2016) TFEB at a glance. *J. Cell Sci.* **129**, 2475–2481
23. Palmieri, M., Impey, S., Kang, H., di Ronza, A., Pelz, C., Sardiello, M., and Ballabio, A. (2011) Characterization of the CLEAR network reveals an integrated control of cellular clearance pathways. *Hum. Mol. Genet.* **20**, 3852–3866
24. Sardiello, M., Palmieri, M., di Ronza, A., Medina, D. L., Valenza, M., Gennarino, V. A., Di Malta, C., Donaudy, F., Embrione, V., Polishchuk, R. S., Banfi, S., Parenti, G., Cattaneo, E., and Ballabio, A. (2009) A gene network regulating lysosomal biogenesis and function. *Science* **325**, 473–477
25. Settembre, C., Di Malta, C., Polito, V. A., Garcia, A. M., Vetrini, F., Erdin, S., Erdin, S. U., Huynh, T., Medina, D., Colella, P., Sardiello, M., Rubinsztein, D. C., and Ballabio, A. (2011) TFEB links autophagy to lysosomal biogenesis. *Science* **332**, 1429–1433
26. Tsunemi, T., Ashe, T. D., Morrison, B. E., Soriano, K. R., Au, J., Roque, R. A., Lazarowski, E. R., Damian, V. A., Masliah, E., and La Spada, A. R. (2012) PGC-1alpha rescues Huntington's disease proteotoxicity by preventing oxidative stress and promoting TFEB function. *Sci. Transl. Med.* **4**, 142r–197r
27. Polito, V. A., Li, H., Martini-Stoica, H., Wang, B., Yang, L., Xu, Y., Swartzlander, D. B., Palmieri, M., di Ronza, A., Lee, V. M., Sardiello, M., Ballabio, A., and Zheng, H. (2014) Selective clearance of aberrant tau proteins and rescue of neurotoxicity by transcription factor EB. *EMBO Mol. Med.* **6**, 1142–1160
28. Dehay, B., Bove, J., Rodriguez-Muela, N., Perier, C., Recasens, A., Boya, P., and Vila, M. (2010) Pathogenic lysosomal depletion in Parkinson's disease. *J. Neurosci.* **30**, 12535–12544
29. Decressac, M., Mattsson, B., Weikop, P., Lundblad, M., Jakobsson, J., and Bjorklund, A. (2013) TFEB-mediated autophagy rescues midbrain dopamine neurons from alpha-synuclein toxicity. *Proc. Natl. Acad. Sci. U. S. A.* **110**, E1817–E1826
30. Hidvegi, T., Stolz, D. B., Alcorn, J. F., Yousem, S. A., Wang, J., Leme, A. S., Houghton, A. M., Hale, P., Ewing, M., Cai, H., Garchar, E. A., Pastore, N., Annunziata, P., Kaminski, N., Pilewski, J., *et al.* (2015) Enhancing autophagy with drugs or lung-directed gene therapy reverses the pathological effects of respiratory epithelial cell proteinopathy. *J. Biol. Chem.* **290**, 29742–29757
31. Pastore, N., Blomenkamp, K., Annunziata, F., Piccolo, P., Mithbaokar, P., Maria, S. R., Vetrini, F., Palmer, D., Ng, P., Polishchuk, E., Iacobacci, S., Polishchuk, R., Teckman, J., Ballabio, A., and Brunetti-Pierri, N. (2013) Gene transfer of master autophagy regulator TFEB results in clearance of toxic protein and correction of hepatic disease in alpha-1-anti-trypsin deficiency. *EMBO Mol. Med.* **5**, 397–412
32. Bartlett, J. J., Trivedi, P. C., Yeung, P., Kienesberger, P. C., and Pulinilkunnil, T. (2016) Doxorubicin impairs cardiomyocyte viability by suppressing transcription factor EB expression and disrupting autophagy. *Biochem. J.* **473**, 3769–3789
33. Trivedi, P. C., Bartlett, J. J., Perez, L. J., Brunt, K. R., Legare, J. F., Hassan, A., Kienesberger, P. C., and Pulinilkunnil, T. (2016) Glucolipotoxicity diminishes cardiomyocyte TFEB and inhibits lysosomal autophagy during obesity and diabetes. *Biochim. Biophys. Acta* **1861**, 1893–1910
34. Godar, R. J., Ma, X., Liu, H., Murphy, J. T., Weinheimer, C. J., Kovacs, A., Crosby, S. D., Saftig, P., and Diwan, A. (2015) Repetitive stimulation of autophagy-lysosome machinery by intermittent fasting preconditions the myocardium to ischemia-reperfusion injury. *Autophagy* **11**, 1537–1560
35. Pan, B., Zhang, H., Cui, T., and Wang, X. (2017) TFEB activation protects against cardiac proteotoxicity via increasing autophagic flux. *J. Mol. Cell. Cardiol.* **113**, 51–62
36. Javaheri, A., Bajpai, G., Picataggi, A., Mani, S., Foroughi, L., Evie, H., Kovacs, A., Weinheimer, C. J., Hyrc, K., Xiao, Q., Ballabio, A., Lee, J. M., Matkovich, S. J., Razani, B., Schilling, J. D., *et al.* (2019) TFEB activation in macrophages attenuates postmyocardial infarction ventricular dysfunction independently of ATG5-mediated autophagy. *JCI Insight* **4**, e127312
37. [preprint] Kenny, H. C., Weatherford Eric, T., Collins, G. V., Allamargot, C., Gesalla, T., Zimmerman, K., Goel, H., McLendon, J. M., Dai, D. F., Romac, T., Streeter, J., Sharafuddin, J., Diwan, A., Pereira, R., Song, L. S., and Abel, E. D. (2021) Cardiac specific overexpression of transcription factor EB (TFEB) in normal hearts induces pathologic cardiac hypertrophy and lethal cardiomyopathy. *bioRxiv*. https://doi.org/10.1101/2021.02.16.431474
38. Wang, H., Wang, R., Carrera, I., Xu, S., and Lakshmana, M. K. (2016) TFEB overexpression in the P301S model of tauopathy mitigates increased PHF1 levels and lipofuscin puncta and rescues memory deficits. *eNeuro*. https://doi.org/10.1523/ENEURO.0042-16.2016
39. Ma, X., Mani, K., Liu, H., Kovacs, A., Murphy, J. T., Foroughi, L., French, B. A., Weinheimer, C. J., Kraja, A., Benjamin, I. J., Hill, J. A., Javaheri, A., and Diwan, A. (2019) Transcription factor EB activation rescues advanced alphaB-crystallin mutation-induced cardiomyopathy by normalizing desmin localization. *J. Am. Heart Assoc.* **8**, e10866
40. Torra, A., Parent, A., Cuadros, T., Rodriguez-Galvan, B., Ruiz-Bronchal, E., Ballabio, A., Bortolozzi, A., Vila, M., and Bove, J. (2018) Overexpression of TFEB drives a pleiotropic neurotrophic effect and prevents Parkinson's disease-related neurodegeneration. *Mol. Ther.* **26**, 1552–1567
41. Liu, Y., Xue, X., Zhang, H., Che, X., Luo, J., Wang, P., Xu, J., Xing, Z., Yuan, L., Liu, Y., Fu, X., Su, D., Sun, S., Zhang, H., Wu, C., *et al.* (2019) Neuronal-targeted TFEB rescues dysfunction of the autophagy-lysosomal

pathway and alleviates ischemic injury in permanent cerebral ischemia. *Autophagy* **15**, 493–509
42. Sun, J., Lu, H., Liang, W., Zhao, G., Ren, L., Hu, D., Chang, Z., Liu, Y., Garcia-Barrio, M. T., Zhang, J., Chen, Y. E., and Fan, Y. (2021) Endothelial TFEB (transcription factor EB) improves glucose tolerance via upregulation of IRS (insulin receptor substrate) 1 and IRS2. *Arterioscler. Thromb. Vasc. Biol.* **41**, 783–795
43. Evans, T. D., Zhang, X., Jeong, S. J., He, A., Song, E., Bhattacharya, S., Holloway, K. B., Lodhi, I. J., and Razani, B. (2019) TFEB drives PGC-1alpha expression in adipocytes to protect against diet-induced metabolic dysfunction. *Sci. Signal.* **12**, eaau2281
44. Kim, J., Kim, S. H., Kang, H., Lee, S., Park, S. Y., Cho, Y., Lim, Y. M., Ahn, J. W., Kim, Y. H., Chung, S., Choi, C. S., Jang, Y. J., Park, H. S., Heo, Y., Kim, K. H., *et al.* (2021) TFEB-GDF15 axis protects against obesity and insulin resistance as a lysosomal stress response. *Nat. Metab.* **3**, 410–427
45. Gottlieb, R. A., Andres, A. M., Sin, J., and Taylor, D. P. (2015) Untangling autophagy measurements: All fluxed up. *Circ. Res.* **116**, 504–514
46. Liang, Q., De Windt, L. J., Witt, S. A., Kimball, T. R., Markham, B. E., and Molkentin, J. D. (2001) The transcription factors GATA4 and GATA6 regulate cardiomyocyte hypertrophy *in vitro* and *in vivo*. *J. Biol. Chem.* **276**, 30245–30253
47. Akazawa, H., and Komuro, I. (2003) Roles of cardiac transcription factors in cardiac hypertrophy. *Circ. Res.* **92**, 1079–1088
48. Kang, C., Xu, Q., Martin, T. D., Li, M. Z., Demaria, M., Aron, L., Lu, T., Yankner, B. A., Campisi, J., and Elledge, S. J. (2015) The DNA damage response induces inflammation and senescence by inhibiting autophagy of GATA4. *Science* **349**, a5612
49. Song, J. X., Sun, Y. R., Peluso, I., Zeng, Y., Yu, X., Lu, J. H., Xu, Z., Wang, M. Z., Liu, L. F., Huang, Y. Y., Chen, L. L., Durairajan, S. S., Zhang, H. J., Zhou, B., Zhang, H. Q., *et al.* (2016) A novel curcumin analog binds to and activates TFEB *in vitro* and *in vivo* independent of MTOR inhibition. *Autophagy* **12**, 1372–1389
50. Wilkins, B. J., Dai, Y. S., Bueno, O. F., Parsons, S. A., Xu, J., Plank, D. M., Jones, F., Kimball, T. R., and Molkentin, J. D. (2004) Calcineurin/NFAT coupling participates in pathological, but not physiological, cardiac hypertrophy. *Circ. Res.* **94**, 110–118
51. Oka, T., Maillet, M., Watt, A. J., Schwartz, R. J., Aronow, B. J., Duncan, S. A., and Molkentin, J. D. (2006) Cardiac-specific deletion of Gata4 reveals its requirement for hypertrophy, compensation, and myocyte viability. *Circ. Res.* **98**, 837–845
52. Yamamura, S., Izumiya, Y., Araki, S., Nakamura, T., Kimura, Y., Hanatani, S., Yamada, T., Ishida, T., Yamamoto, M., Onoue, Y., Arima, Y., Yamamoto, E., Sunagawa, Y., Yoshizawa, T., Nakagata, N., *et al.* (2020) Cardiomyocyte Sirt (Sirtuin) 7 ameliorates stress-induced cardiac hypertrophy by interacting with and deacetylating GATA4. *Hypertension* **75**, 98–108
53. Wang, X., Wang, Q., Li, W., Zhang, Q., Jiang, Y., Guo, D., Sun, X., Lu, W., Li, C., and Wang, Y. (2020) TFEB-NF-kappaB inflammatory signaling axis: A novel therapeutic pathway of dihydrotanshinone I in doxorubicin-induced cardiotoxicity. *J. Exp. Clin. Cancer Res.* **39**, 93
54. Santin, Y., Sicard, P., Vigneron, F., Guilbeau-Frugier, C., Dutaur, M., Lairez, O., Couderc, B., Manni, D., Korolchuk, V. I., Lezoualc, 'H. F., Parini, A., and Mialet-Perez, J. (2016) Oxidative stress by monoamine oxidase-A impairs transcription factor EB activation and autophagosome clearance, leading to cardiomyocyte necrosis and heart failure. *Antioxid. Redox Signal.* **25**, 10–27
55. Wang, K., Zhang, T., Lei, Y., Li, X., Jiang, J., Lan, J., Liu, Y., Chen, H., Gao, W., Xie, N., Chen, Q., Zhu, X., Liu, X., Xie, K., Peng, Y., *et al.* (2018) Identification of ANXA2 (annexin A2) as a specific bleomycin target to induce pulmonary fibrosis by impeding TFEB-mediated autophagic flux. *Autophagy* **14**, 269–282
56. Khalique, O. K., and Bello, N. A. (2019) Are we getting closer to the HEART of hypertensive heart disease? *Hypertension*. https://doi.org/10.1161/HYPERTENSIONAHA.119.13169
57. Sciarretta, S., Yee, D., Nagarajan, N., Bianchi, F., Saito, T., Valenti, V., Tong, M., Del, R. D., Vecchione, C., Schirone, L., Forte, M., Rubattu, S., Shirakabe, A., Boppana, V. S., Volpe, M., *et al.* (2018) Trehalose-induced activation of autophagy improves cardiac remodeling after myocardial infarction. *J. Am. Coll. Cardiol.* **71**, 1999–2010
58. Qi, G. M., Jia, L. X., Li, Y. L., Li, H. H., and Du, J. (2014) Adiponectin suppresses angiotensin II-induced inflammation and cardiac fibrosis through activation of macrophage autophagy. *Endocrinology* **155**, 2254–2265
59. Shi, J., Surma, M., Yang, Y., and Wei, L. (2019) Disruption of both ROCK1 and ROCK2 genes in cardiomyocytes promotes autophagy and reduces cardiac fibrosis during aging. *FASEB J.* **33**, 7348–7362
60. Yan, C. H., Li, Y., Tian, X. X., Zhu, N., Song, H. X., Zhang, J., Sun, M. Y., and Han, Y. L. (2015) CREG1 ameliorates myocardial fibrosis associated with autophagy activation and Rab7 expression. *Biochim. Biophys. Acta* **1852**, 353–364
61. Liu, S., Chen, S., Li, M., Zhang, B., Shen, P., Liu, P., Zheng, D., Chen, Y., and Jiang, J. (2016) Autophagy activation attenuates angiotensin II-induced cardiac fibrosis. *Arch. Biochem. Biophys.* **590**, 37–47